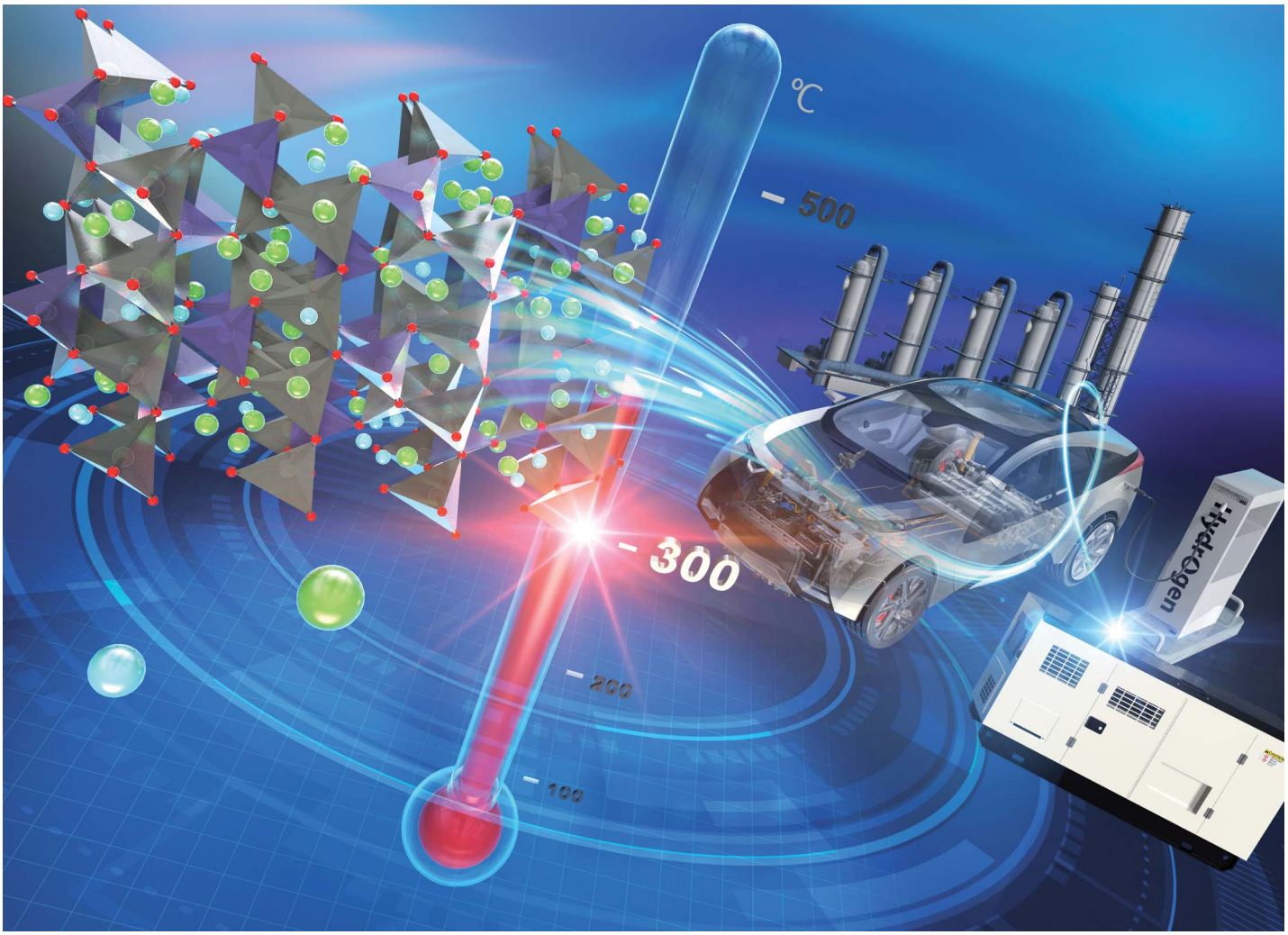

Highlighting a study on intermediate-temperature proton conductivity of Li^+/H^+ ion-exchanged material $(Li,H)_{3.5}Zn_{0.25}GeO_4$ by a group of researchers led by Dr. Toshiaki Matsui from Kyoto University.

Intermediate-temperature proton conductivity of Li^+/H^+ ion-exchanged material $(Li,H)_{3.5}Zn_{0.25}GeO_4$

In this study, we demonstrate the development of novel proton conductors that are operative at intermediate temperatures, especially 300-400 °C, through the simple ion-exchange method. The Li^+/H^+ ion-exchange was conducted for $Li_{14}Zn(GeO_4)_4$ in non-aqueous solutions, and the chemical formula of the resultant sample was determined as $Li_{3.13}H_{0.37}Zn_{0.25}GeO_4$. This material exhibited relatively high electrical conductivity of 39.0 mS cm^{-1} and 5.5 mS cm^{-1} at 300 °C and 200 °C, respectively, in 10% H_2O–90% N_2. Furthermore, the main charge carrier in this electrolyte was identified as a proton from the H/D isotopic exchange study.

As featured in:

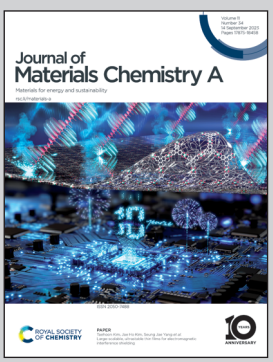

See Toshiaki Matsui *et al.*, *J. Mater. Chem. A*, 2023, **11**, 18207.

ROYAL SOCIETY OF CHEMISTRY

rsc.li/materials-a

Registered charity number: 207890

Journal of Materials Chemistry A

ROYAL SOCIETY OF CHEMISTRY

PAPER

View Article Online
View Journal | View Issue

Open Access Article. Published on 20 July 2023. Downloaded on 12/4/2025 8:51:38 PM.
This article is licensed under a Creative Commons Attribution-NonCommercial 3.0 Unported Licence.

Check for updates

Cite this: J. Mater. Chem. A, 2023, 11, 18207

Intermediate-temperature proton conductivity of Li^+/H^+ ion-exchanged material $(Li,H)_{3.5}Zn_{0.25}GeO_4$†

Toshiaki Matsui, *[a] Takashi Ozeki,[a] Kazunari Miyazaki,[a] Sadahiro Nagasaka,[a] Hiroki Muroyama,[a] Kenichi Imagawa,[b] Yoshimi Okada[b] and Koichi Eguchi[a]

Received 10th April 2023
Accepted 20th July 2023

DOI: 10.1039/d3ta02144k

rsc.li/materials-a

For decades, much effort has been devoted to developing proton conductors applicable to electrochemical devices at intermediate temperatures. However, promising materials that possess sufficient conductivity have not been realized yet. This study demonstrates the development of novel proton conductors that are operative at intermediate temperatures, especially 300–400 °C, through the simple ion-exchange method. The Li^+/H^+ ion-exchange process was conducted for $Li_{14}Zn(GeO_4)_4$, one of the members of lithium super ionic conductors (LISICONs), in non-aqueous solutions. The chemical formula of the resultant sample was determined as $Li_{3.13}H_{0.37}Zn_{0.25}GeO_4$ from instrumental analyses. The electrical conductivity of this material was evaluated to be 87.0 mS cm^{-1}, 39.0 mS cm^{-1}, and 5.5 mS cm^{-1} at 400 °C, 300 °C, and 200 °C, respectively, in 10% H_2O–90% N_2. Furthermore, the main charge carrier in this electrolyte was identified as a proton from the H/D isotopic exchange study. These findings open up the possibility of realizing new electrochemical devices that are operative at 200–400 °C.

1. Introduction

Proton-conducting materials have attracted much attention towards hydrogen economy. Solid-state electrochemical devices employing proton conductors can readily handle hydrogen-involved chemical reactions by controlling the input/output current and/or voltage. Fuel cells, steam electrolyzers, and electrochemical hydrogen pumps, *etc.*, fall under this category. Thus, many researchers have tried to develop proton conductors operating at intermediate temperatures in the range of 250–500 °C.[1–18] From the perspective of electrochemical devices, the intermediate-temperature operation has several advantages, *e.g.*, (i) an ease in temperature control and (ii) applicability of various constituent materials. Most studies are based on the modification of already existing proton conductors. For example, the perovskite-type oxides are the most prominent electrolyte materials among various proton conductors.[4,5,19] Particularly, $BaCeO_3$- and $BaZrO_3$-based oxides exhibit high proton conductivity at *ca.* 600 °C.[20] However, there are some drawbacks, which have to be overcome, including the low chemical stability to CO_2, low sinterability, and hole conductivity in an oxidizing atmosphere.[21–23] Solid acids, such as CsH_2PO_4, are also one of the candidates. Although CsH_2PO_4 undergoes a phase transition at around 230 °C to the super protonic phase for high proton conductivity >10^{-2} S cm^{-1}, the operating temperature range is limited. Furthermore, relatively high humidification, *e.g.*, 0.3 atm at 250 °C, is essential to prevent dehydration.[7,8,24] Thus, at present, there are no materials that are applicable at intermediate temperatures with sufficiently high conductivity *i.e.*, >10^{-2} S cm^{-1}, chemical stability, and ease in sinterability. Therefore, a new class of proton conductors is desired.

Recently, Wei *et al.* reported that the well-known lithium ion conductor of $Li_{14}Zn(GeO_4)_4$-based oxide $Li_{13.9}Sr_{0.1}Zn(GeO_4)_4$ shows proton conductivity at intermediate temperatures after immersion in diluted acetic acid aqueous solutions.[25] Although the Li^+/H^+ ion-exchange for lithium ion conductors has been reported to study the lithium ion mobility in solids,[26–28] they applied this idea to synthesize proton conductors for the first time. The crystal structure of $Li_{14}Zn(GeO_4)_4$ has a rigid three-dimensional framework of $[Li_{11}Zn(GeO_4)_4]^{3-}$ with the remaining three Li^+ ions in interstitial sites.[29] The migration of Li^+ between these interstitial sites results in high Li^+ conductivity. Thus, upon immersion treatment in the acetic acid aqueous solution, Li^+ in interstitial sites can be replaced by H^+. The resultant sample exhibited the proton conductivity of 48 mS cm^{-1} at 600 °C.[25] However, the proton conduction in ion-exchanged $Li_{14}Zn(GeO_4)_4$ is full of obscurity. A follow-up test was then conducted based on their report,[25] and there were some new findings (see Fig. S1 and S2 in the ESI†). After the acetic acid treatment, all of the Li^+ ions in interstitial sites were replaced with H^+ and a part of the $[Li_{11}Zn(GeO_4)_4]^{3-}$ framework

[a]Department of Energy and Hydrocarbon Chemistry, Graduate School of Engineering, Kyoto University, Nishikyo-ku, Kyoto 615-8510, Japan. E-mail: matsui@elech.kuic.kyoto-u.ac.jp

[b]Chiyoda Corporation, Nishi-ku, Yokohama 220-8765, Japan

† Electronic supplementary information (ESI) available: TGA profiles (Fig. S1(a) and S3), XRD patterns (Fig. S1(b)), electrochemical properties (Fig. S2, S5 and S6), Nyquist plots (Fig. S4), lattice parameters (Table S1). See DOI: https://doi.org/10.1039/d3ta02144k

Open Access Article. Published on 20 July 2023. Downloaded on 12/4/2025 8:51:38 PM.
This article is licensed under a Creative Commons Attribution-NonCommercial 3.0 Unported Licence.

appeared to be broken, judging from the thermogravimetric and structural analyses (Fig. S1†). Furthermore, the impurity phase Li_2GeO_3 was formed during the sintering process of pellets at 1150 °C, which resulted in an increase in the electrolyte resistance. Consequently, the ionic conductivity was evaluated to be 11.5 mS cm^{-1} and 0.29 mS cm^{-1} at 600 °C and 400 °C, respectively (Fig. S2(b)†). Therefore, the Li^+/H^+ ion-exchange in aqueous solutions is inappropriate to synthesize proton conductors with high performance.

In this study, we applied the new ion-exchange procedure to achieve both high proton conductivity and structural stability upon the sintering process. The Li^+/H^+ ion-exchange for $Li_{14}Zn(GeO_4)_4$ was conducted in non-aqueous solutions, and the resultant sample $(Li,H)_{3.5}Zn_{0.25}GeO_4$ exhibited significantly high conductivity.

2. Experimental

2.1 Powder preparation and characterization

The powder of $Li_{14}Zn(GeO_4)_4$ was synthesized by the solid-state reaction. A stoichiometric amount of Li_2CO_3 (FUJIFILM Wako Pure Chemical Corporation), ZnO (FUJIFILM Wako Pure Chemical Corporation), and GeO_2 (Sigma-Aldrich, Co.) was ball-milled with ethanol for 24 h. The obtained mixture was dried on a hot-plate to evaporate ethanol, and then pelletized into a cylindrical shape. The pellet was calcined at 1150 °C for 5 h in air, followed by pulverization. This process for the solid-state reaction was repeated twice. The resultant sample was denoted as Pristine LZG. The Li^+/H^+ exchange for Pristine LZG was performed in an *N*,*N*-dimethylformamide (FUJIFILM Wako Pure Chemical Corporation) solution dissolved with benzoic acid (FUJIFILM Wako Pure Chemical Corporation) for 24 h at room temperature. A mass of 2.5 g of Pristine LZG powder was immersed in 200 mL of 20 mM benzoic acid–*N*,*N*-dimethylformamide solution. The ion-exchanged powder was collected by the filtration and washed with *N*,*N*-dimethylformamide. After that, the resultant powder was dried in a vacuum oven at 130 °C.

For the phase identification, X-ray diffraction analysis was carried out for powder samples using an Ultima IV X-ray diffractometer (Rigaku) with Cu Kα radiation.

Thermogravimetric analysis (TGA) was conducted to estimate the amount of ion exchange under flowing air with a heating rate of 10 °C min^{-1} (Rigaku, Thermoplus TG8120). The electrolyte composition was also analyzed by inductively coupled plasma optical emission spectrometer (ICP-OES, ThermoFisher SCIENTIFIC iCAP7000).

2.2 Electrochemical measurements

For electrochemical measurements, ion-exchanged samples were pelletized into a cylindrical shape or rectangular parallelepiped shape and cold-isostatically pressed at 300 MPa, followed by sintering at 1150 °C for 5 h in air. Sputtered Au and Au wire were used as electrodes. The dc four-probe method was applied to measure the electrical conductivity. The ac impedance analysis was also conducted in a frequency range of 1 MHz to 0.1 Hz at an applied voltage amplitude of 10 mV using an impedance analyzer (Solartron 1260A equipped with 1287A potentiostat). Measurements were conducted in a heating process (from 200 °C to 450 °C) in humidified atmospheres by bubbling the gas (N_2, H_2, O_2) through water at desired temperatures. Deuterated water was also used to study the isotopic effect (H/D). Prior to the conductivity measurements, sintered samples were annealed at 200 °C for 12 hours in experimental atmospheres.

The apparent transference number of proton, $\bar{t}_{H^+}$, was calculated from the electromotive force of the hydrogen concentration cell. A silver paste (Fujikura Kasei Co. Ltd, D-550) was applied as the electrodes for the pelletized sample (2.0 mm-thick); in this case, the paste was printed and heated at 900 °C for 1 h in air. The diameter of the electrodes was 6 mm. The cell was set between alumina tubes and then sealed by Pyrex glass rings sputtered with gold. A gaseous mixture of 5% H_2O–x% H_2–(95 – x)% N_2 (gas(I)) was supplied to one side, and 5% humidified hydrogen (5% H_2O–95% H_2, gas(II)) was flowed to the other side. The theoretical electromotive force, E_{th}, was calculated by the following Nernstian equation;

$$E_{th} = \frac{RT}{2F}\ln\frac{P_{H_2}(\text{gas II})}{P_{H_2}(\text{gas I})} \quad (1)$$

where R, T, F, and P_{H_2} are the gas constant, temperature, Faraday constant, and partial pressure of hydrogen, respectively. The apparent transference number of proton was determined as follows;

$$\bar{t}_{H^+} = \frac{E}{E_{th}} \quad (2)$$

The OCV measurement in the fuel cell condition was also conducted at 400 °C for the cell with the following configuration: 5% humidified hydrogen, Pd|$(Li,H)_{3.5}Zn_{0.25}GeO_4$ (1.8 mm-thick)|Ag, 5% humidified oxygen. The experimental setup is the same as for the electromotive force measurement.

3. Results and discussion

3.1 Characteristics of materials ion-exchanged in non-aqueous solutions

TGA profiles for Pristine LZG ($Li_{3.5}Zn_{0.25}GeO_4$) and Li^+/H^+ ion-exchanged LZG in a 20 mM benzoic acid–*N*,*N*-dimethylformamide solution ($(Li,H)_{3.5}Zn_{0.25}GeO_4$, hereafter abbreviated as H-LZG) are shown in Fig. 1(a). For H-LZG, a weight loss observed in the heating process was ascribable to the elimination of protons in the lattice. This indicates that the Li^+/H^+ ion-exchange proceeded successfully in a non-aqueous solution. The chemical composition of H-LZG was roughly estimated by assuming that protons in the lattice were evaporated in the form of steam. In this calculation, the weight loss up to 600 °C was used because the influence of the CO_2 desorption was included above 700 °C, which will be probably related to the thermal decomposition of carbonates. The exchange ratio of Li^+ ions in interstitial sites was 49.7%, judging from the fact that the weight loss was 1.92% from room temperature up to 600 °C.

Open Access Article. Published on 20 July 2023. Downloaded on 12/4/2025 8:51:38 PM.
This article is licensed under a Creative Commons Attribution-NonCommercial 3.0 Unported Licence.

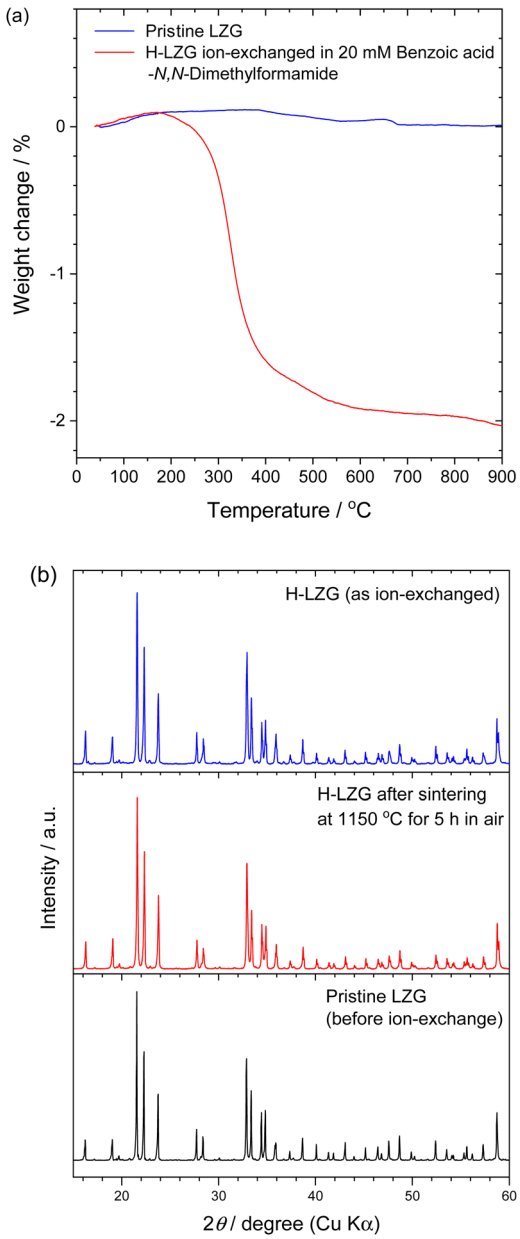

Fig. 1 (a) TGA profiles of Pristine LZG and H-LZG, measured in air at the heating rate of 10 °C min^{-1}. (b) XRD patterns of H-LZG before and after sintering in air and Pristine LZG.

This estimation was verified by ICP-OES; the amount of lithium, zinc, and germanium ions in the filtrate was analyzed quantitatively. Only lithium ion was detected in the filtrate, indicating that lithium ions were successfully exchanged for protons without leaching other cations. It should be noted that the weight loss estimated from ICP-OEC was almost comparable to that obtained from TGA, with a difference in a weight loss percentage of 0.1%. Thus, TGA provided the amount of Li^+/H^+ ion-exchange with relatively high accuracy. This result was different from that obtained by ion-exchange treatment in 5 mM acetic acid aqueous solution (Fig. S1†). In the aqueous solution, Li^+ ions in interstitial sites were fully exchanged and some part of the three-dimensional framework of $[Li_{11}Zn(GeO_4)_4]^{3-}$ also appeared to be dissolved.

Interestingly, the weight loss percentage up to 600 °C after immersion in non-aqueous solutions with a benzoic acid converged to *ca.* 1.9 wt% even though the ion-exchange treatment was conducted in various conditions by changing the temperature, concentration, and solvent (Fig. S3†). This means that H-LZG can reach the stable state with a chemical composition of $Li_{3.13}H_{0.37}Zn_{0.25}GeO_4$ (the exchange ratio of Li^+ ions in interstitial sites: 49.2%), regardless of the ion-exchange condition. From XRD analysis (Fig. 1(b) and Table S1†), it was revealed that H-LZG maintained the initial skeletal structure of Pristine LZG. This will reflect the progress of Li^+/H^+ partial substitution in interstitial sites, as is expected. It should be noted that even after the sintering process at 1150 °C, the secondary phase was not detected. Thus, we succeeded in the establishment of an excellent ion-exchange procedure.

3.2 Electrochemical properties of H-LZG

Fig. 2(a) shows the temperature dependence of electrical conductivity for various electrolytes measured at 200–450 °C in 10% H_2O–90% N_2. In Fig. S4,† typical Nyquist plots of the H-LZG electrolyte are also provided. The intercept with the real axis in the high frequency region was assigned to the bulk resistance, which was plotted as AC conductivity in Fig. 2(a). It should be noted that the electrical conductivity measured by DC method was a little bit lower than that by AC method (Fig. 2(b)). This is because the resistance derived from the DC method is the sum of bulk and grain boundary resistances. The electrical conductivity of H-LZG was 87.0 mS cm^{-1}, 39.0 mS cm^{-1}, and 5.5 mS cm^{-1} at 400 °C, 300 °C and 200 °C, respectively. These values are higher than those for Pristine LZG, indicating that protons with relatively high mobility were incorporated into the lattice by the ion-exchange treatment. The humidity dependence of conductivity was very slight in the range of 3–10% (see Fig. 3). Thus, it is verified that to maintain the proton concentration in the electrolyte, humidification should be performed within the range where the dehydration reaction is suppressed. Furthermore, the conductivity was almost independent of gaseous atmospheres. Thus, this material is applicable as an ion-conductive electrolyte to a wide range of oxygen partial pressures, such as fuel cell operating conditions. Such a conductivity dependence on gaseous atmospheres is different from that observed in $BaCeO_3$- and $BaZrO_3$-based oxides. Pristine LZG has two different Li^+ interstitial sites with 55% and 16% occupancies. According to the DFT calculation for the proton transport mechanism in ion-exchanged LZG, protons can migrate through these interstitial sites within the three-dimensional Li^+ transport network.[25] Therefore, proton conduction in H-LZG is expected to occur by the same mechanism, in which about half of the Li^+ ions located in the interstitial sites are exchanged.

However, there was a possibility for the migration of both Li^+ and H^+. Then, the H/D isotopic exchange was conducted for the

Open Access Article. Published on 20 July 2023. Downloaded on 12/4/2025 8:51:38 PM.
This article is licensed under a Creative Commons Attribution-NonCommercial 3.0 Unported Licence.

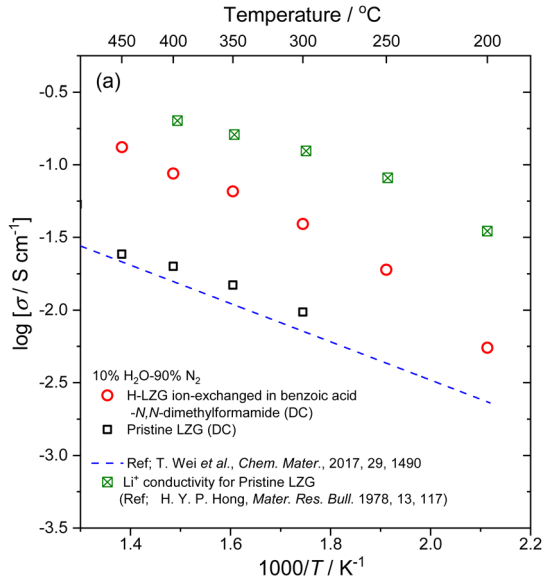

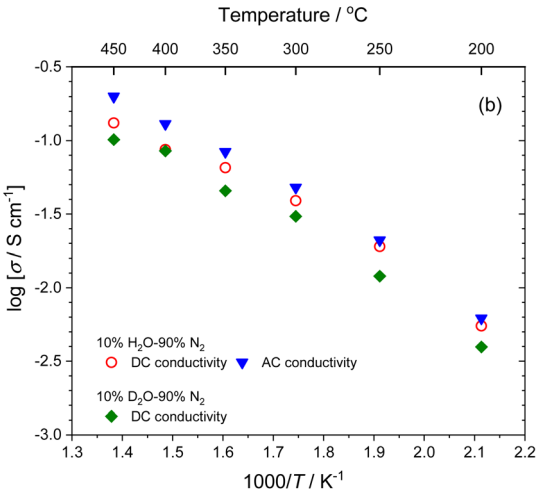

Fig. 2 (a) Temperature dependence of electrical conductivity as a function of reciprocal temperature for H-LZG in 10% H_2O–90% N_2. Some data were referred from ref. 25 and 30. (b) Electrical conductivity of H-LZG measured by AC and DC methods in 10% H_2O–90% N_2 and 10% D_2O–90% N_2. Arrhenius plots are shown in Fig. S5(a) and (b).†

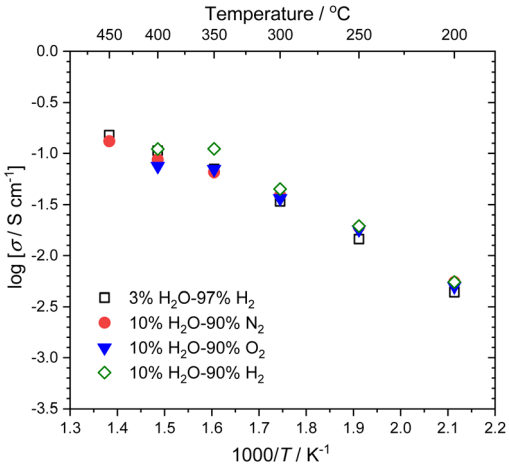

Fig. 3 Temperature dependence of electrical conductivity as a function of reciprocal temperature for H-LZG in various atmospheres.

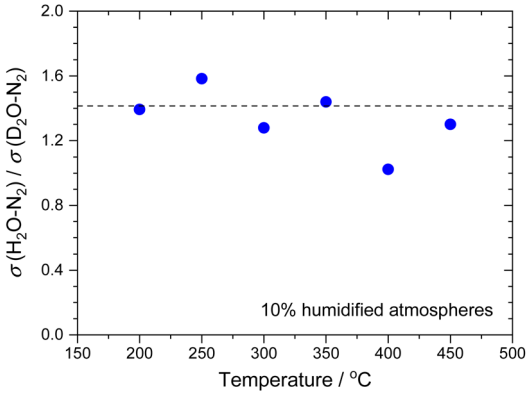

Fig. 4 The ratio of electrical conductivity for H-LZG in 10% H_2O–90% N_2 and 10% D_2O–90% N_2 as a function of temperature (DC method). Arrhenius plots are shown in Fig. S6.†

H-LZG electrolyte to identify the main migration carrier in the electrolyte. Fig. 4 displays the ratio of ionic conductivity in 10% H_2O–90% N_2 and 10% D_2O–90% N_2 as a function of temperature, which is calculated from the results in Fig. 2(b). As is expected, the conductivity in 10% H_2O–90% N_2 was higher than that in 10% D_2O–90% N_2. Moreover, the $\sigma(H_2O\text{–}N_2)/\sigma(D_2O\text{–}N_2)$ ratio was close to the theoretical ratio of $\sqrt{2}$,[31] which originates from the difference in the mass of the proton and deuteron. Thus, the main charge carrier in H-LZG was determined to be the proton at the temperatures investigated. However, the conductivity ratio appears to decrease as the temperature increases. This tendency should correspond to the decrease in the charge carrier, proton, in H-LZG due to the dehydration at higher temperatures, especially >400 °C.

3.3 Electrochemical behavior and structural stability of H-LZG in reducing atmospheres

Fig. 5(a) shows the time course of ionic conductivity in 3% humidified hydrogen at 300 °C. It is apparent that the conductivity decreased gradually with the elapse of time, suggesting the degradation of H-LZG. The same behavior was confirmed in both humidified hydrogen and nitrogen atmospheres at 300 °C and 400 °C. Then, the crystalline structure after exposure to a reducing atmosphere was studied, as displayed in Fig. 5(b) and (c). Although the main peaks ascribable to H-LZG were maintained after heat treatment, the formation of the Li_4GeO_4 phase was confirmed at both 300 °C and 400 °C. This indicates the progress of phase separation, leading to the reduction in ionic conductivity. Considering that the formation of the Li_4GeO_4 phase was more gradual at 300 °C, the operating temperature is one of the key factors to maintain the structure and conductivity as well. A series of observed phenomena can be predictable from the phase diagram of Pristine LZG, which is the solid solution of Li_4GeO_4–Zn_2GeO_4.[29] Pristine LZG with the

Open Access Article. Published on 20 July 2023. Downloaded on 12/4/2025 8:51:38 PM.
This article is licensed under a Creative Commons Attribution-NonCommercial 3.0 Unported Licence.

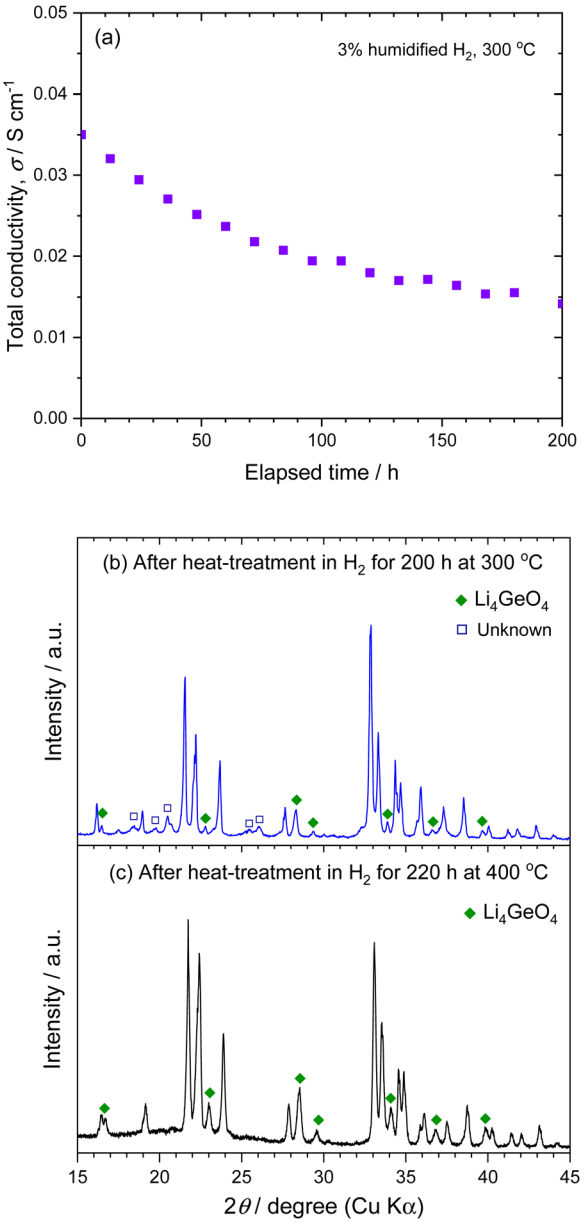

Fig. 5 (a) Time course of the ionic conductivity in 3% humidified hydrogen at 300 °C. XRD patterns of the H-LZG powder after exposure to non-humidified hydrogen at (b) 300 °C and (c) 400 °C.

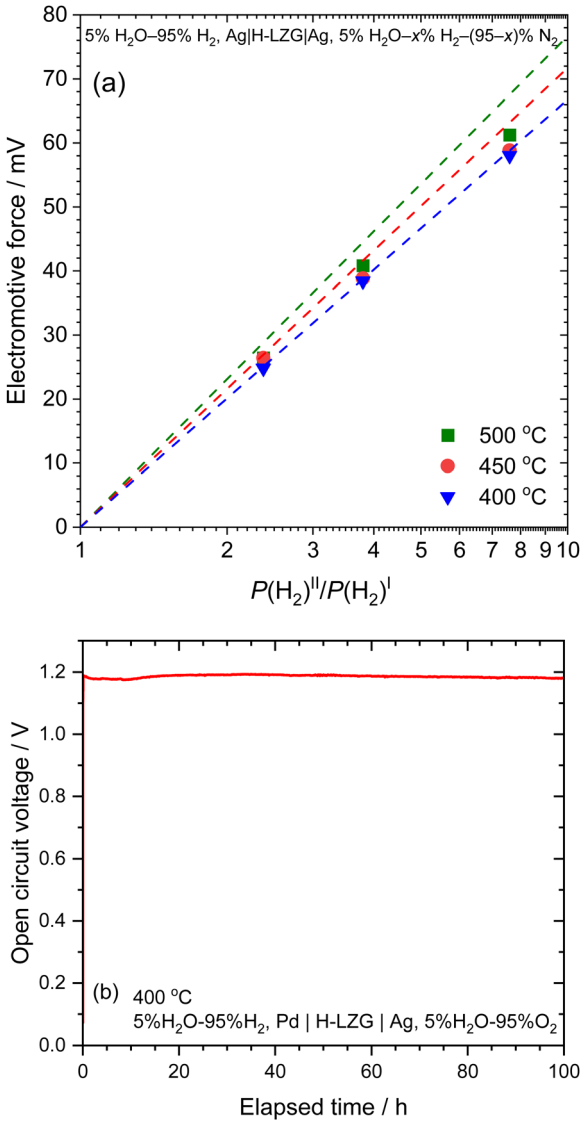

Fig. 6 (a) Nernstian potential of a hydrogen concentration cell, 5% H_2O–95% H_2, Ag|H-LZG|Ag, 5% H_2O–x% H_2–(95 − x)% N_2. (b) Time course of open circuit voltage at 400 °C for the cell, 5% H_2O–95% H_2, Pd|H-LZG|Ag, 5% H_2O–95% O_2.

chemical composition selected in this study is the γ_{II}-solid solution above *ca.* 600 °C, while the segregation of the Li_4GeO_4 phase from the solid solution proceeds below this temperature. Thus, the substitutional doping of aliovalent cations may be an effective way to achieve both structural stability and ionic conductivity. In the near future, we will report on the related materials.

Finally, the Nernstian potential of a hydrogen concentration cell with the H-LZG electrolyte at 400–500 °C is summarized in Fig. 6(a). Within the measurement time of this experiment, the degradation of the electrolyte can be ignored. Unfortunately, it was difficult to obtain the results below 350 °C due to the absence of appropriate sealants. Broken lines correspond to the theoretical values at each temperature. The apparent transference number of proton was evaluated to be 0.98, 0.90, and 0.89 at 400 °C, 450 °C, and 500 °C, respectively. The deviation of the apparent transference number from unity at higher temperatures can be mainly attributed to two reasons. One is the reduction in the apparent transference number of proton due to the lithium ion conduction, as expected from Fig. 4. The other is the gas leakage. The time course of open circuit voltage (OCV) was also measured at 400 °C in the fuel cell condition while supplying humidified hydrogen and oxygen to the anode and cathode, respectively, as shown in Fig. 6(b). The OCV measured was 1.18 V, which was almost identical to the theoretical value, and constant even after 100 h of holding. This result indicates that the protons can migrate through the electrolyte, although phase separation proceeded with time at 400 °

Open Access Article. Published on 20 July 2023. Downloaded on 12/4/2025 8:51:38 PM.
This article is licensed under a Creative Commons Attribution-NonCommercial 3.0 Unported Licence.

C. Therefore, the series of Li^+/H^+ ion-exchanged LISICONs will be promising proton conductors at intermediate temperature if they can escape thermodynamic constraints.

4. Conclusions

This is the first report for the development of a novel proton conductor that is operative at intermediate temperatures. In this study, a simple ion-exchange method with non-aqueous solutions was applied for $Li_{14}Zn(GeO_4)_4$. In this case, almost half of the lithium ions located in the interstitial sites were exchanged to protons, regardless of ion-exchange conditions. The resultant material $Li_{3.13}H_{0.37}Zn_{0.25}GeO_4$ (H-LZG) achieved high ionic conductivity of 87.0 mS cm^{-1}, 39.0 mS cm^{-1}, and 5.5 mS cm^{-1} at 400 °C, 300 °C, and 200 °C, respectively, in 10% H_2O–90% N_2. Since the main charge carrier in H-LZG was determined to be the proton, this material is applicable as a proton conductor at intermediate temperatures. On the other hand, there are still drawbacks to be settled for the realization of new electrochemical devices, such as fuel cells and electrolyzers. One is the thermal stability of H-LZG at intermediate temperatures. The other is the development of high-performance electrodes, which are compatible with chemical stability with an electrolyte.

Author contributions

T. M. led the development of the concept, guided the experimental design, and supervised the research. T. O. developed the materials and performed the following experiments and analyses: XRD, thermogravimetry, conductivity. K. M. conducted the same experiments described above for samples ion-exchanged in aqueous solutions. S. N. conducted the transference number and OCV measurements. K. I. and Y. O. discussed the electrical conductivity and stability of developed material, and its application to practical devices. H. M. and K. E. provided critical suggestions for experimental and analytical methods. T. M. wrote the paper with contributions from all authors.

Conflicts of interest

There are no conflicts to declare.

Acknowledgements

This paper is based on results obtained from the projects commissioned by the New Energy and Industrial Technology Development Organization (NEDO) and JSPS KAKENHI Grant Number JP20H02841 (Grant-in-Aid for Scientific Research (B)).

References

1 T. Norby, *Solid State Ionics*, 1999, **125**, 1.
2 B. C. H. Steele and A. Heinzel, *Nature*, 2001, **414**, 345.
3 A. I. Baranov, B. V. Merinov, A. V. Tregubchenko, V. P. Khiznichenko, L. A. Shuvalov and N. M. Schagina, *Solid State Ionics*, 1989, **36**, 279.
4 H. Iwahara, T. Esaka, H. Uchida and N. Maeda, *Solid State Ionics*, 1981, **3–4**, 359.
5 H. Iwahara, H. Uchida, K. Ono and K. Ogaki, *J. Electrochem. Soc.*, 1988, **135**, 529.
6 N. Ito, M. Iijima, K. Kimura and S. Iguchi, *J. Power Sources*, 2005, **152**, 200.
7 D. A. Boysen, T. Uda, C. R. I. Chisholm and S. M. Haile, *Science*, 2004, **303**, 68.
8 S. M. Haile, C. R. I. Chisholm, K. Sasaki, D. A. Boysen and T. Uda, *Faraday Discuss.*, 2007, **134**, 17.
9 T. Matsui, T. Kukino, R. Kikuchi and K. Eguchi, *J. Electrochem. Soc.*, 2006, **153**, A339.
10 T. Matsui, T. Noto, H. Muroyama, M. Iijima and K. Eguchi, *J. Power Sources*, 2011, **196**, 9445.
11 M. Nagao, T. Kamiya, P. Heo, A. Tomita, T. Hibino and M. Sano, *J. Electrochem. Soc.*, 2006, **153**, A1604.
12 T. Shimura, S. Fujimoto and H. Iwahara, *Solid State Ionics*, 2001, **143**, 117.
13 G. Kojo, R. Tsukimura and J. Otomo, *Solid State Ionics*, 2017, **306**, 89.
14 C. C. Duan, J. H. Tong, M. Shang, S. Nikodemski, M. Sanders, S. Ricote, A. Almansoori and R. O'Hayre, *Science*, 2015, **349**, 1321.
15 M. C. Verbraeken, C. Cheung, E. Suard and J. T. S. Irvine, *Nat. Mater.*, 2015, **14**, 95.
16 T. Yamaguchi, S. Tsukuda, T. Ishiyama, J. Nishii, T. Yamashita, H. Kawazoe and T. Omata, *J. Mater. Chem. A*, 2018, **6**, 23628.
17 J. Hyodo, K. Kitabayashi, K. Hoshino, Y. Okuyama and Y. Yamazaki, *Adv. Energy Mater.*, 2020, **10**, 2000213.
18 T. Murakami, J. R. Hester and M. Yashima, *J. Am. Chem. Soc.*, 2020, **142**, 11653.
19 L. Malavasi, C. A. J. Fisher and M. S. Islam, *Chem. Soc. Rev.*, 2010, **39**, 4370.
20 D. A. Medvedev, J. G. Lyagaeva, E. V. Gorbova, A. K. Demin and P. Tsiakaras, *Prog. Mater. Sci.*, 2016, **75**, 38.
21 P. Sawant, S. Varma, B. N. Wani and S. R. Bharadwaj, *Int. J. Hydrogen Energy*, 2012, **37**, 3848.
22 H. Shimada, X. Li, A. Hagiwara and M. Ihara, *J. Electrochem. Soc.*, 2013, **160**, F597.
23 D. Han, S. Uemura, C. Hiraiwa, M. Majima and T. Uda, *ChemSusChem*, 2018, **11**, 4102.
24 C. S. Gittleman, H. Jia, E. S. D. Castro, C. R. I. Chisholm and Y. S. Kim, *Joule*, 2021, **5**, 1660.
25 T. Wei, L. A. Zhang, Y. Chen, P. Yang and M. Liu, *Chem. Mater.*, 2017, **29**, 1490.
26 L. Truong and V. Thangadurai, *Chem. Mater.*, 2011, **23**, 3970.
27 L. Sebastian, R. S. Jayashree and J. Gopalakrishnan, *J. Mater. Chem.*, 2003, **13**, 1400.
28 L. Truong and V. Thangadurai, *Inorg. Chem.*, 2012, **51**, 1222.
29 P. G. Bruce and A. R. West, *Mater. Res. Bull.*, 1980, **15**, 379.
30 H. Y. P. Hong, *Mater. Res. Bull.*, 1978, **13**, 117.
31 A. S. Nowick and A. V. Vaysleyb, *Solid State Ionics*, 1997, **97**, 17.

 This journal is © The Royal Society of Chemistry 2023